

Giant Magnetoresistance in Carbon Nanotubes with Single-Molecule Magnets TbPc₂

Igor V. Krainov,^{†,‡} Janina Klier,^{¶,§} Alexander P. Dmitriev,[†] Svetlana Klyatskaya,[¶] Mario Ruben,^{¶,||} Wolfgang Wernsdorfer,^{¶,⊥,#} and Igor V. Gornyi^{*,¶,†,§}

[†]Ioffe Institute of the Russian Academy of Sciences, 194021 St. Petersburg, Russia

[‡]Lappeenranta University of Technology, P.O. Box 20, 53851 Lappeenranta, Finland

[¶]Institut für Nanotechnologie, Karlsruhe Institute of Technology, 76021 Karlsruhe, Germany

[§]Institut für Theorie der Kondensierten Materie, Karlsruhe Institute of Technology, 76128 Karlsruhe, Germany

^{||}Institut de Physique et Chimie des Materiaux (IPCMS), CNRS-Université de Strasbourg, 67034 Strasbourg, France

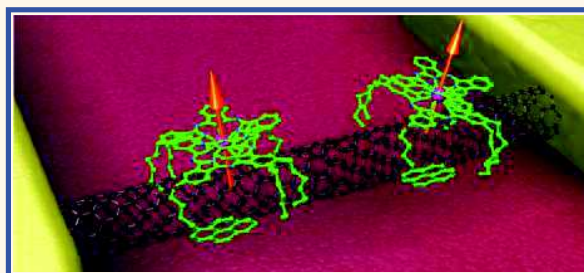
[⊥]Physikalisches Institut, Karlsruhe Institute of Technology, 76128 Karlsruhe, Germany

[#]Institut Néel, CNRS and Université Grenoble Alpes, 38000 Grenoble, France

Supporting Information

ABSTRACT: We present experimental results and a theoretical model for the gate-controlled spin-valve effect in carbon nanotubes with side-attached single-molecule magnets TbPc₂ (Terbium(III) bis-phthalocyanine). These structures show a giant magnetoresistance up to 1000% in experiments on single-wall nanotubes that are tunnel-coupled to the leads. The proposed theoretical model combines the spin-dependent Fano effect with Coulomb blockade and predicts a spin–spin interaction between the TbPc₂ molecules, mediated by conducting electrons *via* the charging effect. This gate-tuned interaction is responsible for the stable magnetic ordering of the inner spins of the molecules in the absence of magnetic field. In the case of antiferromagnetic arrangement, electrons with either spin experience the scattering by the molecules, which results in blocking the linear transport. In strong magnetic fields, the Zeeman energy exceeds the effective antiferromagnetic coupling and one species of electrons is not scattered by molecules, which leads to a much lower total resistance at the resonant values of gate voltage, and hence to a supramolecular spin-valve effect.

KEYWORDS: carbon nanotubes, TbPc₂, magnetic molecules, supramolecular spin-valve effect, giant magnetoresistance, Coulomb blockade



Molecular spintronics^{1–6} encompasses the abilities to characterize, manipulate, and read out the molecular spin states of nanosystems down to the single-molecule level. Further device miniaturization and the need to effectively interface organic and inorganic materials for biomedical and nanoelectronic applications are the driving forces to this field.⁷ Single-molecule functionality on short time scales can be realized^{8–16} by using state-of-the-art optical and electronic techniques.

More specifically, single-molecule magnets (SMM) provide a promising way to realize nanometer-scale structures with a stable spin orientation.⁵ SMMs are formed by an inner magnetic core with organic ligands as a surrounding shell.^{17,18} The ligands can be tailored to bind them on surfaces or into molecular junctions.^{19–24} Delocalized bonds in SMMs, which can enhance their conducting properties, often have the function to strengthen magnetic interactions of the core ions. The variety of shapes and sizes of SMMs as well as the

possibility of selective substitution of ligands can conveniently customize the coupling of SMMs to the environment.²⁵ Moreover, the magnetic properties can be changed without modifying the structure by replacing the magnetic ions in SMMs.²⁶ Although the deposition of SMMs on surfaces or between leads may affect their magnetic properties,^{25,27} in the sense of their low structural versatility, SMMs prevail over nonmolecular nanosystems which typically show large size and anisotropy distributions. Compared to magnetic nanoparticles, SMMs have crucial advantages that they are extremely monodisperse and can be investigated in molecular crystals.

Importantly, SMMs unify the archetypal macroscale properties of a magnet with quantum features of a nanoscale object. An impressive variety of quantum effects in SMMs, observable

Received: March 23, 2017

Accepted: June 14, 2017

Published: June 14, 2017

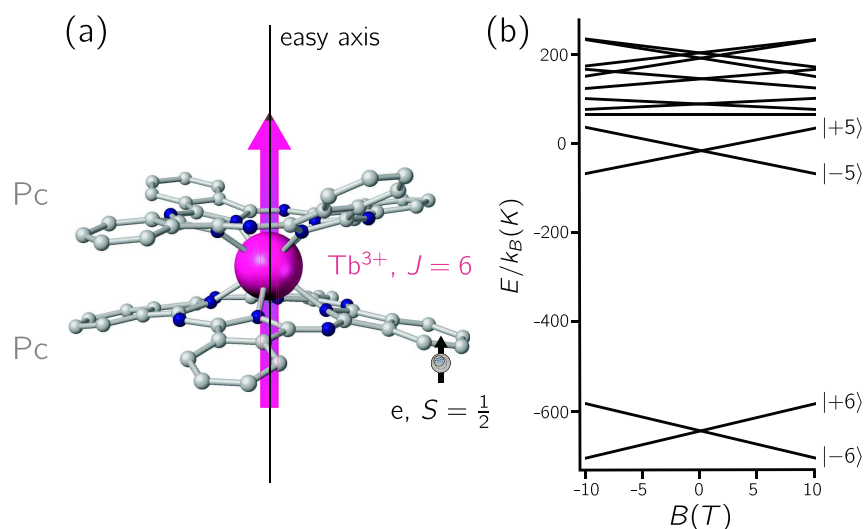


Figure 1. (a) Scheme of the single molecule magnet TbPc_2 . The spins of the ion ($J = 6$) and the “resident” electron on the ligands ($S = 1/2$) are shown by the pink and black arrows. (b) Energy diagram of TbPc_2 in external magnetic field applied in the direction of the easy axis. The ground state has two spin projections ± 6 .

up to very high temperatures thanks to the progress in molecular designs, ranges from Berry-phase interference and quantum coherence to quantum tunneling of magnetization. While the study of SMMs has already led to strong impact on spintronics,³ yet more striking results are expected in the course of further developing design of devices based on individual SMMs.

In contact with nanostructures, SMMs may strongly modify their transport properties. A remarkable example of such an effect is the giant magnetoresistance (GMR) that was observed in a carbon nanotube (CNT) with side-attached magnetic molecules TbPc_2 .^{10,28,29} The GMR effect has great potential for different applications, for example, sensors, magnetic memory, and others. Materials with GMR are characterized by the size of the structure and the ratio $[G(B) - G(0)]/G(0)$, where $G(B)$ and $G(0)$ denote the conductance with and without magnetic field, respectively. Reproducible sharp jumps of the conductance of the CNTs tunnel-coupled to the leads were observed with a slow variation of magnetic field that oriented the magnetic moments of the molecules parallel to each other. Varying the gate voltage, the GMR effect in nanotubes can reach 1000%. By its manifestations, this spin-valve effect is similar to the phenomenon of GMR in thin metal films with magnetic contacts, which, in turn, is one of the most prominent and widely used in practice phenomena in the field of spintronics. A similar spin-valve effect was observed in thin graphene strips with SMMs³⁰ and in CNTs with permalloy contacts.³¹

Nanostructures involving SMMs, such as molecular quantum dots coupled to metallic leads, were addressed theoretically in a number of works. In particular, a possible read-out for the local spin orientation *via* the measurement of the spin current,³² asymmetries in the Coulomb diamonds and Kondo peaks,³³ and the spin-blockade effect associated with a change of magnetic anisotropy³⁴ were discussed. For a single-wall CNT with a single side-attached molecule, it has been argued that the tunnel magnetoresistance may depend on the exchange interaction between the CNT and the SMM.³⁵ In ref 36, a mechanism of the spin-valve effect for (effectively infinite) CNTs with SMMs was proposed. However, the GMR and

peculiar nonlinear transport observed experimentally in tunnel-coupled CNTs with several SMMs still lack a comprehensive theoretical explanation.

In this paper, we discuss both the experimental and theoretical aspects of electronic transport through CNTs with side-attached TbPc_2 SMMs. We propose a theoretical model that accounts for the interplay of the following main ingredients: (i) spin-dependent resonant scattering of conducting electrons on the bound state inside a molecule (Fano resonance)^{36–38} and (ii) Coulomb blockade³⁹ inside the CNT. Specifically, the electronic states on molecules give rise to the spin-dependent resonant suppression of the transmission of conducting electrons. The Coulomb interaction between electrons inside the nanotube leads to Coulomb blockade, with the linear transport blocked for the antiparallel orientation of molecule spins at all values of gate voltage. The developed theory predicts a long-range interaction between SMMs, which is responsible for the stable magnetic ordering of the inner spins of the molecules, and explains the GMR in nanotubes with TbPc_2 molecules.

Remarkably, the sign and the strength of the molecular spin–spin interaction can be varied by the gate voltage, thus implying that the arrangement of SMMs spins and, more generally, the magnetic properties of supramolecular nanostructures can be efficiently manipulated by external gates. This gate-controlled spin-valve effect allows designing SMM-based devices with engineered local gates. Demonstration of a superior flexibility of chemistry with respect to the tuning and controlling the properties of the molecules (spin, anisotropy, redox potential, response to light and electrical field, *etc.*) is expected to lead to further breakthroughs in the field of quantum electronics and spintronics.

RESULTS AND DISCUSSION

Structure of Single-Molecule Magnets. In this work, we focus on the particular SMM, TbPc_2 double decker, see Figure 1(a). The TbPc_2 molecule consists of a terbium(III) ion with $4f^8$ electrons in the inner shell, which have a total angular momentum 3 and a total spin 3. The metal ion is coordinated by an organic ligand possessing an easy axis. Strong spin–orbit

coupling leads therefore to a total angular momentum $J = 6$. At low temperatures, the magnetic moment of terbium has only two projections on the easy axis, $J_z = \pm 6$, because of a strong magnetic anisotropy caused by interaction⁴⁰ with the two phthalocyanine (Pc) ligands, Figure 1(b).

In addition, terbium has a nuclear spin $3/2$, leading to a hyperfine interaction with electrons of the inner shell. The nuclear spin of SMM can be effectively read out by conductance measurements^{40,41} on a structure where TbPc_2 is directly coupled to the leads. This hyperfine interaction can be controlled by applying a gate voltage.⁴² Terbium spin J can change its projection through the spin-phonon coupling.⁴³ Furthermore, quantum Einstein–de Haas effect⁴⁴ was observed with these molecules.

The phthalocyanine ligands in TbPc_2 possess an electronic state with spin $S = 1/2$.¹⁸ Due to a strong Coulomb interaction between particles with opposite spins,¹⁴ only one spin orientation is occupied.⁴⁵ This localized spin S is coupled by the exchange interaction⁴² to the terbium spin J of $4f$ electrons.

Experimental Results. In this Section, we outline the most salient experimental findings showing the giant magneto-resistance effect in the linear transport through a CNT, as well as the peculiar differential conductance in the regime of Coulomb blockade.

In Figure 2, we present a typical conductance measurement performed in magnetic field that was varied in time at the fixed

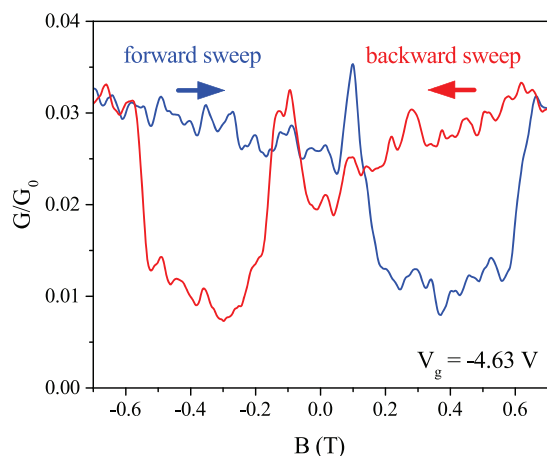


Figure 2. Linear-response conductance at fixed gate voltage $V_g = -4.63$ V in units of quantum conductance G_0 as a function of dynamically swept magnetic field (sweep rate: 0.07 T/s). Blue curve: forward sweep from -0.7 to 0.7 T; red curve: backward sweep.

gate voltage ($V_g = -4.63$ V) and vanishing source-drain voltage (linear response, $V_{sd} \rightarrow 0$). The sweep rate of magnetic field is 70 $\text{mT}\cdot\text{s}^{-1}$. The blue curve shows the conductance for increasing B from negative values to positive and the red curve for the sweep in the opposite direction.

The asymmetry of the conductance jumps with respect to $B \rightarrow -B$ is caused by the finite sweep rate. At negative magnetic fields, the ground spin state of Tb is $J_z = +6$, see Figure 1(b). For a sufficiently fast sweep of magnetic field, the molecule spin continues residing on the $J_z = +6$ branch, which at positive magnetic fields corresponds to an excited state, until a relaxation process takes place that flips the Tb spin. The main source of relaxation is associated with the spin-phonon coupling in TbPc_2 molecule.⁴³ At the same time, for relatively

low sweep rate, quantum tunneling of magnetization by Landau–Zener mechanism becomes important.²⁸

The maps of the differential conductance in units of conductance quantum $G_0 = e^2/h$ as a function of source-drain and gate voltage are shown in Figure 3 for zero magnetic field

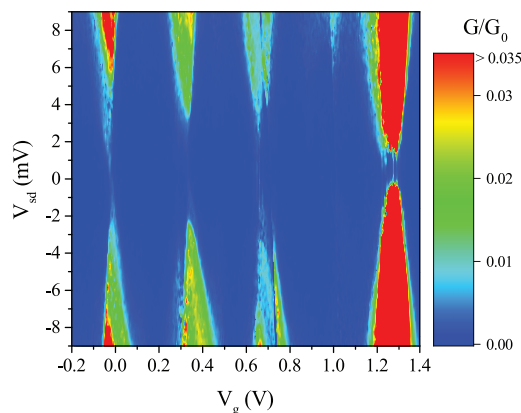


Figure 3. Coulomb blockade maps at zero magnetic field in the plane of source-drain voltage V_{sd} and gate voltage V_g . The differential conductance $G = dI/dV_{sd}$ is given in units of quantum conductance G_0 .

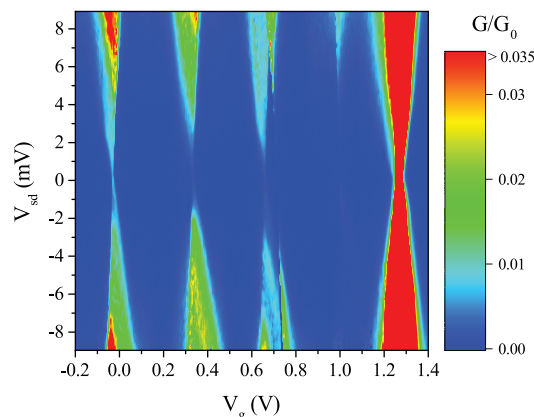


Figure 4. Coulomb blockade maps as in Figure 3, now in a static magnetic field, $B = 1$ T.

and in Figure 4 for the static magnetic field, $B = 1$ T. The measurements were performed by sweeping the source-drain voltage V_{sd} at a given value of the gate voltage V_g and then changing V_g . Coulomb diamonds in these maps indicate the presence of Coulomb blockade caused by strong electron–electron interaction between electrons in CNT. From the extrapolation of Coulomb diamonds we estimate the charging energy in CNT as $E_C \approx 20$ meV. Another important observation is that the conduction regions are rather homogeneous, which indicates that the broadening of single-particle energy levels in the CNT is relatively strong.

Remarkably, at zero magnetic field (Figure 3), the conductance at zero V_{sd} is suppressed for all values of V_g and the transport gap $\delta V_{sd} \sim 1 \div 2$ meV is observed.¹⁰ This is in contrast to the conventional CB maps in quantum dots,⁴⁶ where the linear conductance is finite at resonant values of V_g . In the CB map obtained for strong magnetic field (Figure 4),

the transport gaps are closed at certain values of the gate voltage. This fact is emphasized by the zoom pictures of the Coulomb blockade map for the gate voltage range near $V_g \sim 1.25$ V in Figure 5 (zero B) and Figure 6 ($B = 1$ T).

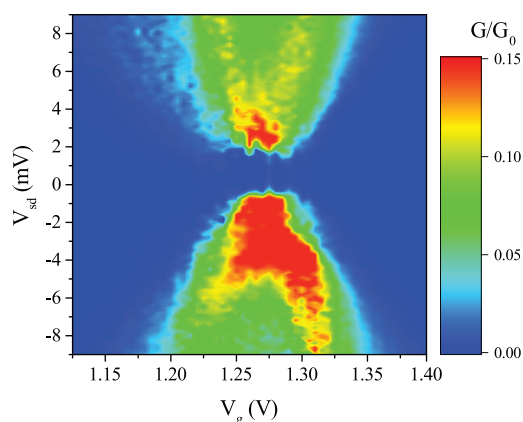


Figure 5. Zoom into Coulomb blockade map around $V_g = 1.25$ at zero magnetic field. The differential conductance is given in units of G_0 .

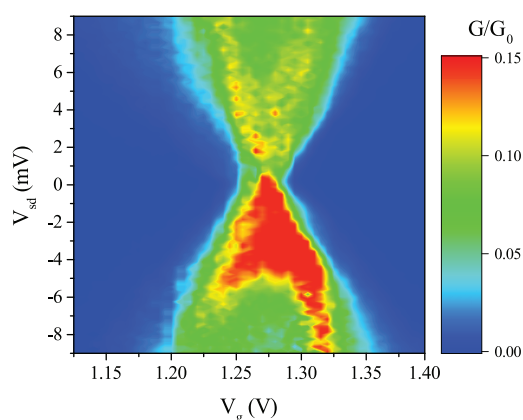


Figure 6. Zoom into Coulomb blockade map around $V_g = 1.25$ at $B = 1$ T.

In Figure 7, we present the conductance as a function of the source-drain voltage at fixed gate voltage $V_g = 1.27$ V with and without static magnetic field. This plot demonstrates the GMR effect of the order of 1000%: the conductance drops from $G(B = 1 \text{ T}) = 0.14 G_0$ to $G(B = 0) = 0.006 G_0$. We note in passing that the center of the low-conductance window is shifted from $V_{sd} = 0$ to the right by $0.5 \div 1$ meV.

Apart from the GMR observed at $V_g = 1.25 \div 1.3$ V, another important experimental feature is a weaker spin-valve effect for other values of the gate voltage in Figures 3 and 4, for example, for $V_g = 0.335$ V, as demonstrated in Figure 8. Both with and without magnetic field, the linear conductance is of the same order as the zero-field conductance in Figure 7. We emphasize, however, that the zero- B linear conductance in Figure 8 is still lower than the conductance at $B = 1$ T. Thus, we arrive at the conclusion that the experimentally observed magnetoresistance depends on the gate voltage, *i.e.*, is a gate-controlled supramolecular spin-valve effect. Note also, that the region of suppressed conductance (the “transport gap”) in Figure 8 is narrower for $B = 1$ T.

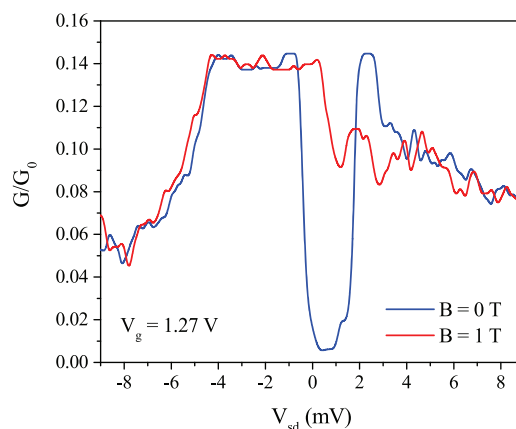


Figure 7. Conductance as a function of the source-drain voltage V_{sd} at fixed gate voltage $V_g = 1.27$ V in units of G_0 . Blue curve: $B = 0$; red curve: $B = 1$ T.

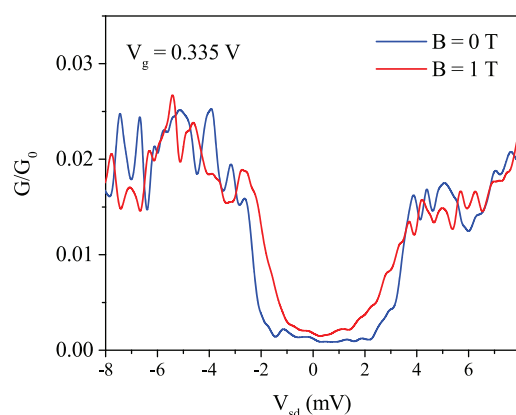


Figure 8. Conductance as a function of the source-drain voltage V_{sd} at fixed gate voltage $V_g = 0.335$ V in units of G_0 . Blue curve: $B = 0$; red curve: $B = 1$ T.

It is worth noting that a similar gate dependence of the magnitude of spin-valve effect can be found already in ref 10. Specifically, in Figures 2a and 2b of ref 10, one can see the strong spin-valve effect (GMR) at gate voltages $V_g = -4.6$ V and $V_g = 2.6$ V, where the transport gap closes in strong magnetic field. For other values of gate voltages in Figures 2a and 2b of ref 10, *e.g.*, at $V_g = -4.4$ V, a weak spin-valve effect was observed, with a transport gap in the CB map apparently persisting also in strong B . In what follows, we will explain the origin of GMR and the gate dependence of the molecular spin-valve effect.

Theoretical Model. Fano Resonance in a Double-Barrier Structure. The TbPc_2 SMM has a delocalized state on its ligands which was observed by Raman measurements⁴⁷ and found in various density-functional calculations.^{36,45} When SMMs are attached to the CNT, tunneling takes place between the electronic states of the CNT and the state localized on ligands and these states hybridize. The hybridization of conduction electrons with a localized state leads to the Fano resonance,^{36–38} which strongly affects the transport through the CNT with side-attached molecules.

To introduce this phenomenon, we first consider the case of one-dimensional electrons with parabolic spectrum in a one-dimensional infinite channel (Figure 9). Electrons in the channel are tunnel-coupled to a single localized state with

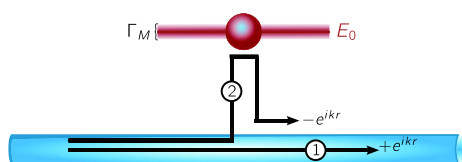


Figure 9. Schematic illustration of the origin of the Fano resonance in transmission through an infinite one-dimensional channel (tube) with a tunnel-coupled localized state (red level) on a molecule. The destructive interference of waves passing the molecule without visiting it (path 1) and visiting the Fano state (path 2) leads to a vanishing transmission for electrons with the resonant energy ($E_k = E_0$).

energy E_0 on the side-attached molecule. The level localized on the molecule acquires a finite broadening Γ_M because of the coupling between the CNT and the molecule. The transmission coefficient for electrons with wave-vector k (energy E_k) through such a system³⁸ is presented in [Supporting Information](#). The scattering off the localized state suppresses the transmission through the channel in the energy window $E_k \sim (E_0 - \Gamma_M, E_0 + \Gamma_M)$.

The Fano blocking of the transport by the side-attached molecule is due to the destructive interference of the electronic wave that passes directly without scattering and the wave that visits the molecule and jumps back to the channel (paths 1 and 2 in [Figure 9](#), respectively). Exactly at the resonance $E_k = E_0$, the scattering phase for path 2 is π , which leads to zero transmission (the sum of the two waves vanishes: $e^{ikx} + e^{ikx+i\pi} = 0$). Accordingly, the reflection coefficient reaches maximum (unity) at the resonance. As a result, the side-attached level acts as an effective barrier whose transparency depends on the energy of scattered electrons.

The importance of Fano resonances for transport through a nanotube with SMMs was pointed out in [ref 36](#). However, the consideration of that paper was restricted to the case of infinite (no tunnel coupling to the leads) systems and hence did not describe the full set of the experimental observations. As we are going to show below, the crucial ingredient of the theoretical model is Coulomb blockade caused by the charge quantization in a finite-length CNT with sufficiently high contact resistance.

In the next step, we calculate the transmission coefficient of a nanotube of length L coupled to the leads, in the presence of a Fano state (upper panel in [Figure 10](#)). The two barriers that separate the nanotube from the leads are characterized by the transmission and reflection coefficients $\mathcal{T}_{L,R}$, $\mathcal{R}_{L,R} = 1 - \mathcal{T}_{L,R}$ (here the subscript “L” stands for the left barrier, “R” for the right). The Fabry–Pérot-type interference inside the CNT leads to the Breit–Wigner resonances in the transmission through the structure at energies corresponding to the quantization energy for infinite barriers.

To illustrate the physics of the double-barrier system with the Fano state, it is instructive to consider the classical case, when dephasing (see [Supporting Information](#)) between barriers is sufficiently strong so that the single-particle levels inside the nanotube overlap. At the same time, we assume that the typical time \hbar/Γ_M that a particle spends on the localized Fano state is shorter than the dephasing time and hence the Fano quantum interference is not destroyed. The transmission coefficient \mathcal{T}_{BMB} for the structure “barrier–molecule–barrier” (BMB) can be calculated in a classical manner with the use of the quantum expression for the transmission and reflection amplitudes (see [Supporting Information](#)) of the Fano state on the molecule:

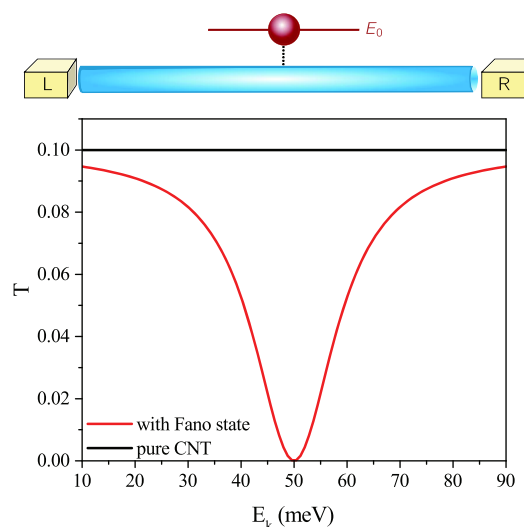


Figure 10. (Upper panel) Schematic illustration of the Fano setup with the one-dimensional channel coupled to the leads by tunneling barriers. (Lower panel) Transmission coefficient for this setup as a function of the carrier energy E_k in the classical case (strong dephasing). The red curve shows the transmission \mathcal{T}_{BMB} for the structure with barriers and one molecule, the black one shows the transmission for two barriers without the molecule (\mathcal{T}_{BB}). The chosen parameters are as follows: the energy of the localized state is $E_0 = 50$ meV; the transmission coefficients across the contacts to the leads are $\mathcal{T}_L = \mathcal{T}_R = 0.17$; the hybridization of conducting electrons with the Fano state is characterized by $\Gamma_M = 30$ meV.

$$\mathcal{T}_{\text{BMB}} = \mathcal{T}_{\text{BB}} \frac{(E_k - E_0)^2}{(E_k - E_0)^2 + \mathcal{T}_{\text{BB}} \Gamma_M^2} \quad (1)$$

$$\mathcal{T}_{\text{BB}} = \frac{\mathcal{T}_L \mathcal{T}_R}{1 - \mathcal{R}_R \mathcal{R}_L} \quad (2)$$

The equation for \mathcal{T}_{BB} describes the classical transmission for the two barriers without molecule, see the [Supporting Information](#). In comparison with the infinite channel, the effect of the two barriers in [eq 1](#) manifests itself in the two aspects. First, the energy window of suppressed transmission due to Fano effect reduces to $E_k \sim (E_0 - \sqrt{\mathcal{T}_{\text{BB}} \Gamma_M}, E_0 + \sqrt{\mathcal{T}_{\text{BB}} \Gamma_M})$. Second, the resulting transmission probability \mathcal{T}_M is multiplied by the transmission coefficient for the two barriers, \mathcal{T}_{BB} . In the lower panel in [Figure 10](#), the classical transmission coefficient for the CNT with one Fano center is presented.

In the general case of arbitrary dephasing (including the zero-dephasing case), the structure of the total transmission probability \mathcal{T}_{BMB} is similar to [eq 1](#) in the sense that the double-barrier transmission coefficient is modulated by the Fano-resonance envelope. For the case of symmetric barriers, the transmission coefficient of the whole structure is presented in [Supporting Information](#). The analysis of the general solution is relegated to future work. What is important for us is that the presence of the Fano state substantially suppresses the transmission through the whole system in the range of energies $E_k \sim (E_0 - \Gamma_0, E_0 + \Gamma_0)$ around E_0 of the width Γ_0 controlled by both the strength of the coupling Γ_M and the transmission probability \mathcal{T}_{BB} for the two barriers. In the presence of two and more molecules, the overall picture remains the same: in the range of Fano-resonance energies, the transmission is strongly

suppressed. In other words, the molecules can be considered as strong barriers for electrons in this energy range. At the same time, away from the Fano resonance, molecules do not essentially affect the transport.

Including Spin: Splitting of Fano Resonances. Let us now discuss the role of the electron and molecule spins in the transport through the CNT-SMM structure. Localized electronic states on Pc ligands of the SMM are characterized by a large Coulomb energy U_0 . Another important fact is the presence of ferromagnetic exchange interaction⁴² between electrons localized on ligands and $4f$ electrons of terbium. The exchange interaction is described by

$$\hat{V}_{\text{ex}} = A(\mathbf{J} \cdot \hat{\mathbf{S}}) \quad (3)$$

where \mathbf{J} and \mathbf{S} are the spins of terbium and of localized electrons, respectively. The exchange interaction constant A has a value of around -0.2 meV. In this case, we can write the energy of spin-up and spin-down electrons on Pc (E_{\uparrow} and E_{\downarrow} , respectively) as

$$E_{\uparrow,\downarrow} = E_0 \pm AJ_z/2 + U_0n_{\uparrow,\downarrow} \quad (4)$$

Due to the strong repulsive Coulomb interaction U_0 , tunneling into TbPc_2 is hardly possible for an electron if the SMM has been already occupied by an electron of opposite spin. The direction of the spin of a localized electron is determined by the spin of Tb *via* the exchange interaction. The orientation of the terbium spin itself is discussed later. Due to magnetic anisotropy of the SMMs, we can fix the magnetic moment of the molecule in one direction and analyze its effect on electron scattering. A schematic diagram illustrating these aspects is presented in Figure 11.

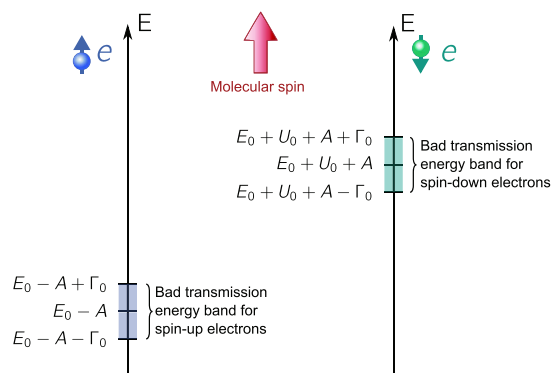


Figure 11. Schematic diagram of electron scattering on TbPc_2 . When a spin-up electron occupies the localized state on the ligand, two regions of bad transmission for electrons are formed due to exchange interaction with Tb spin.

The transmission of an electron through a molecule with given spin J depends on electron's energy and spin. In what follows, we assume the following hierarchy of the energy scales in our model:

$$\Delta \ll E_C \lesssim \Gamma_0 \ll U_0 \quad (5)$$

Here, Δ is the level spacing of these levels and $E_C \sim e^2/L$ is the Coulomb interaction energy between the electrons in the CNT. For the CNT length $L \sim 300$ nm, the single-particle level spacing is about $\Delta \sim 1 \div 2$ meV, and the Coulomb charging energy is $E_C \sim 15 \div 20$ meV. The Fano level broadening $\Gamma_0 \sim 10 \div 20$ meV can be estimated from the conductance map of

transport through a single molecule.⁴² This means that a few levels of size quantization fall into in region with bad transmission. The value of the repulsive Coulomb energy on Pc ligands, $U_0 \sim 100$ meV, was calculated in ref 45.

If the Fermi level is located, for example, in the energy band of poor transmission for electrons with spin-up orientation (see the left part of Figure 11), a single molecule splits the nanotube into two quantum dots (QDs) for this type of carriers. Indeed, for spin-up electrons near the Fermi level (*i.e.*, for those electrons that are involved in transport) there are three barriers: two tunneling barriers connecting the CNT to the source and drain contacts and the effective barrier created by the molecule. At the same time, spin-down carriers near the Fermi level are unaffected by the presence of the single molecule and hence feel only the two outer tunneling barriers that form a single QD.

For the minimal model of two molecules, we therefore encounter a "spin-valve effect" emerging because of the spin-dependent Fano resonances, similar to the one described in ref 36. Specifically, for the antiparallel orientation of the two SMM spins, conducting electrons with either spin projection experience the resonant backscattering by the SMM and the transport is suppressed for all electrons. When the two molecular spins are parallel, conducting electrons with one spin projection see the two Fano barriers inside the CNT and are blocked even stronger. However, electrons with the opposite spin are not affected by either of the molecules, which should lead to a higher conductance of the system.

The difference between our model and that of ref 36 is in the presence of strong tunneling barriers separating the CNT and the leads. As a result, the CNT can be considered as a sequence of quantum dots whose number depends on the spins of carriers and molecules. Specifically, the parallel orientation of the two SMM spins in Figure 11 results in the breaking the CNT into three QDs for the spin-up carriers, while the spin-down carriers feel only one QD. For the antiparallel SMM spins, both spin-down and spin-up carriers see two QDs, being blocked by one of the molecules.

The splitting of the CNT into quantum dots is depicted in Figure 12. Hereinafter, we assume that the Fermi level is located in the lower energy band in Figure 11, *i.e.*, the

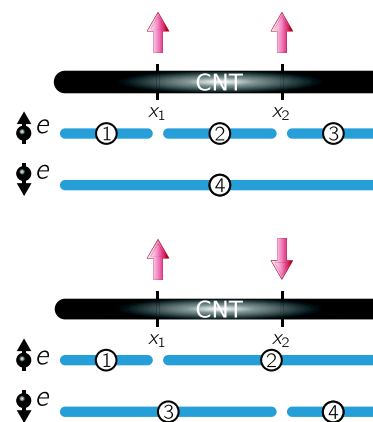


Figure 12. Scheme of quantum dots for electrons in the CNT with energies close to the Fermi energy. The CNT effectively breaks into quantum dots depending on spin orientation of the electrons and molecules. The Fermi level lies in the region of bad transmission for the parallel carrier and SMM spins.

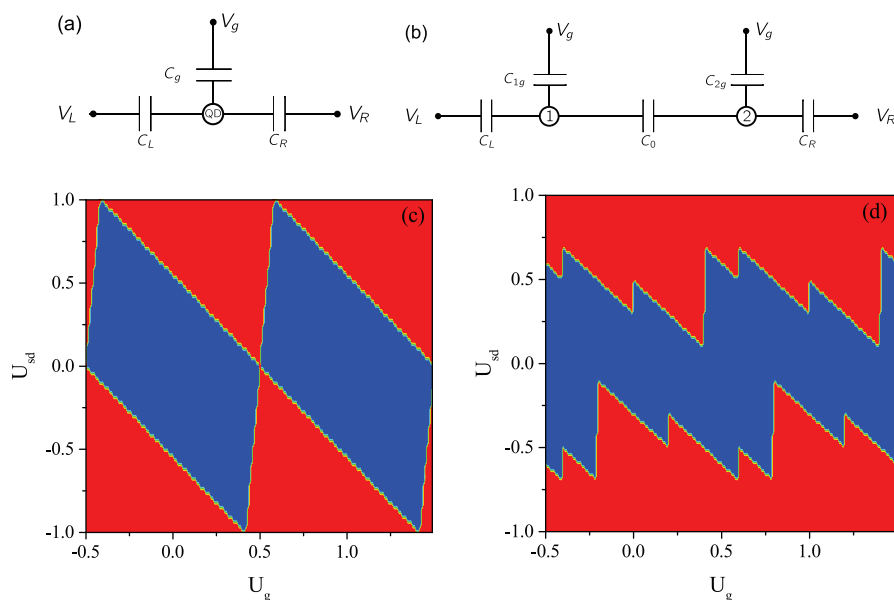


Figure 13. (a) Equivalent electrostatic scheme for a single quantum dot; (b) Equivalent electrostatic scheme for a double quantum dot; (c) and (d) Typical Coulomb-blockade maps for the single and double quantum dots, respectively, at $T = 0$. Blue and red regions correspond to the zero and finite current, respectively.

transmission through the SMMs is suppressed for carriers with the spin parallel to the molecule spin. This assumption can be satisfied by varying gate voltage if the capacitances of the CNT and the molecule are not identical.

It is important to emphasize that the simple picture with the suppression of the transmission by spin-dependent Fano resonances presented at Figure 12 cannot explain all the experimentally observable phenomena without the inclusion of the Coulomb interaction. The presence of several QDs in the system strongly affects the transport properties of the structure because of the charging effects characteristic of Coulomb blockade. In particular, as we are going to show below, the Coulomb interaction gives rise to magnetic ordering of SMM spins in zero magnetic field, which is necessary for the explanation of the spin-valve effect. Below, the interaction effects are analyzed in detail.

Coulomb Blockade. Including Coulomb Interaction. As has been discussed in the previous section, SMMs may split the CNT into several QDs and the Coulomb interaction between electrons, as well as the charge quantization in the QDs, should become important for the transport properties of the structure. Coulomb blockade (CB) was observed in pure CNTs (see, e.g., ref 48) and needs to be taken into account in the analysis of transport in nanotubes with magnetic molecules. Due to CB, the conductance is strongly suppressed for certain ranges of the gate voltage V_g and of the source-drain voltage V_{sd} , as seen in the CB maps in Figures 3 and 5. Below we construct the CB maps for our model where the configuration of QDs in the CNT is determined by spins of SMMs.

Before going into the discussion of the role of CB in transport through CNTs with magnetic molecules, we remind the reader the basics of CB in the simplest case of a single quantum dot. The Coulomb interaction in a finite electronic system is responsible for the emergence of the energy scale E_C referred to as the charging energy. In the process of electron tunneling into the quantum dot, the energy conservation condition involves this interaction energy. As a consequence,

transport through a quantum dot can be blocked by the Coulomb interaction: in order to pass through the dot, an electron should overcome the charging energy. The phenomenon of CB can be described by means of an equivalent electrostatic scheme,³⁹ where the charging energy is encoded by introducing the capacitors, as illustrated for a single quantum dot in Figure 13a.

Quantitatively, the CB effects are characterized by the free energy of the system.⁴⁹ For a single quantum dot it reads (for the zero source-drain voltage V_{sd}) as

$$F_1(N, V_g) = \frac{(eN + C_g V_g)^2}{2(C_g + C_L + C_R)} \quad (6)$$

where N is the number of electrons on the dot, C_g is the capacitance between the dot and the gate, and $C_{L,R}$ are the capacitances between the dot and the leads. In the linear-response regime, *i.e.*, for $V_{sd} \rightarrow 0$, by changing the number of electrons in the QD, one gets generically different values of the free energy,

$$F_1(N) < F_1(N + 1), \quad F_1(N - 1)$$

and electrons cannot tunnel across the QD.

For certain “resonant” values of the gate voltage V_g^* , however, the addition of an extra electron to the QD does not lead to the change in the free energy: $F(N, V_g^*) = F(N + 1, V_g^*)$. The linear conductance through the QD is finite for these values of V_g . For a finite source-drain voltage, the resonant conditions for the free energy of the system are described by the boundaries of the “Coulomb diamonds” in the Coulomb map, with forbidden (Coulomb-blocked) regions shown in blue color in Figure 13c. When the change of N in the course of tunneling to and from the QD is allowed by the energy conservation at a finite source-drain voltage, the current through the system can be finite (red regions in Figure 13c).

We now turn to the crucial difference between the CB transport through a single QD and two or more QDs, which is

a cornerstone of the strong spin-valve effect in our setup. For a system consisting of more than one QD, the conditions for the boundaries of CB diamonds are rather complex. Generically, Coulomb maps for a double-dot system^{49,50} (see the equivalent scheme in Figure 13b) show finite transport gaps around zero source-drain voltage for all values of V_g . In other words, the red regions above and below $V_{sd} = 0$ do not touch each other (the blue regions are not separated from each other unlike in Figure 13c) as illustrated in Figure 13d, where we present a typical Coulomb map for two QDs.

The main difference between the single-dot and double-dot systems is that, in the latter case, to contribute to the overall current an electron needs to tunnel to the first QD, then to the second QD, and then to the lead. As a result, the transport conditions for the double QD should account for the difference in energies for adding an electron to the first and second dot and for the possibility of electron tunneling between the two dots. A finite linear-response conductance at $V_{sd} \rightarrow 0$ requires equal free energies F_2 for configurations with different numbers of particles in QDs:

$$F_2(N_1, N_2, V_g) = F_2(N_1 + 1, N_2, V_g) = F_2(N_1, N_2 + 1, V_g) \quad (7)$$

It is known^{49,50} that double-dot systems can show no transport gap only in the fully symmetric setup: any asymmetry fully blocks linear transport at zero temperature. In a generic case, the conditions (eq 7) are not fulfilled and hence a transport gap opens for a double QD at all values of the gate voltage. By varying the gate voltages, the differences between the free energies in eq 7 can be minimized, which establishes the magnitude of transport gaps $e\delta V_{sd} = \Delta F_{2\text{dots}}$ as a function of V_g , see Figure 13d.

To obtain the CB maps for the CNT with two SMMs, one needs to calculate the free energy^{39,49} of configurations with different molecular spin orientations (parallel, $\uparrow\uparrow$, and antiparallel, $\uparrow\downarrow$) shown in Figure 12. We express the free energy as a function of the number of electrons in the QDs, $\{N\}_i = \{N_1, N_2, N_3, N_4\}$, the gate and source-drain voltages, the charging energy E_C , and a dimensionless function $\phi_{\alpha\beta}$ with $\alpha = \uparrow, \downarrow$, $\beta = \uparrow, \downarrow$:

$$\begin{aligned} F_{\alpha\beta}(\{N\}_i, V_g, V_{sd}) &= E_C \phi_{\alpha\beta} \left(\{N\}_i, \frac{eV_g}{E_C}, \frac{eV_{sd}}{E_C} \right) \\ &= E_C \phi_{\alpha\beta}(\{N\}_i, U_g, U_{sd}) \end{aligned} \quad (8)$$

where U_g, U_{sd} denote the dimensionless gate and source-drain voltages (measured in units of $E_C = e^2/L$). Furthermore, all the capacitances are normalized to the CNT length $C_i \rightarrow C_i/L$. The positions of the two molecules, x_1, x_2 , belong to the range (0, 1). We present the derivation and the explicit expressions for $\phi_{\uparrow\uparrow}$ and $\phi_{\uparrow\downarrow}$ in Supporting Information.

The capacitances that are associated with the gate are proportional to QD length, $C_{ig} \sim l_i$, while the capacitances between the QDs and leads are determined by the spatial overlap between them, $C_{iR,L} \sim l_{R,L}$ (in experiment, the metallic contacts cover the ends of the CNT). The capacitances between the QDs with different spins are determined by their spatial overlap. The capacitances between the QDs in the channel with the same electron spin are written as $C_{ij} \simeq \kappa l_i l_j / (l_i + l_j)$. Here we use a phenomenological parameter κ that characterizes the electrostatic properties of the molecules and can be determined by atomistic numerical simulations of a

SMM attached to the CNT. In what follows, we will use κ as the only fitting parameter of the model.

The significance of parameter κ can be understood in terms of the difference between a single-dot and double-dot system. The double-dot energy $F_2(N_1, N_2)$ in the limit $\kappa \rightarrow \infty$ reduces to the energy of a single-dot system, $F_1(N_1 + N_2)$ with $C_g = C_{1g} + C_{2g}$. Therefore, the fitting parameter associated with capacitances between molecules needs to be large $\kappa \sim 20 \div 30$. Experimental values of the transport gaps $\delta V_{sd} \sim 1 \div 2$ meV $\ll E_C$ are small compared to the charging energy, thus justifying the assumption that $\kappa \gg 1$. The calculated gaps, $\delta(eV_{sd}) = E_C \delta U_{sd} \sim 1 \div 2$ meV, are in a good agreement with the experimental observation. Hereinafter, we take for the capacitors associated with the leads $l_{L,R} = 0.2$, but the results are not too sensitive to this parameter.

Figures 14 and 15 illustrate the CB for antiparallel and parallel spins of molecules, respectively, for the two molecules

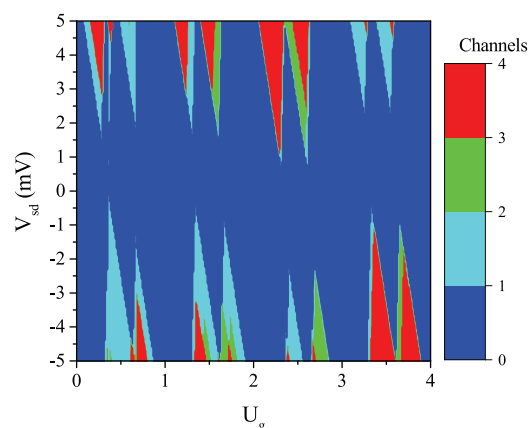


Figure 14. Calculated current map $I(V_g, V_{sd})$ at zero magnetic field in terms of current channels. Positions of molecules: $x_1 = 0.2$, $x_2 = 0.6$; $\kappa = 25$.

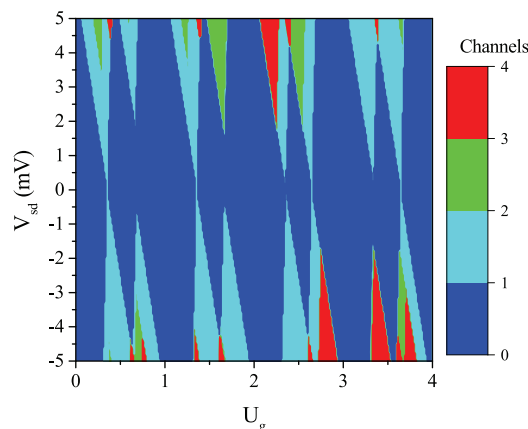


Figure 15. Calculated current map $I(V_g, V_{sd})$ at magnetic field above critical B_c for the same parameters as in Figure 14.

located at $x_1 = 0.2$ and $x_2 = 0.6$. We obtain the regions where current can flow in terms of the current channels, see Supporting Information. We introduce the function $I(V_g, V_{sd})$, which indicates how many distinct configurations $\{N\}_i$ of electron numbers in QDs participate in transport. The function $I(V_g, V_{sd})$ is equal to zero if there are no conducting

states (transport is blocked) and equal to an integer number, $I = M \geq 1$ otherwise, where M is the number of configurations $\{N\}_i$ contributing to the current (the number of open current channels).

One sees in Figure 14 that for the antiparallel spin orientation of the molecules there is a gap around $V_{sd} = 0$ for all values of the gate voltages V_g . This is analogous to the presence of the transport gap for a double-dot system, see Figure 13d. Indeed, as discussed above, for each spin projection of electrons the CNT breaks into two QDs, see the lower panel in Figure 12.

In the case of CNT with SMMs having the parallel molecular spin orientation (upper panel in Figure 12), transport gaps are closed at some values of V_g as for the single-dot CB, Figure 13c. Thus, at such values of the gate voltage one encounters a strong spin-valve effect. However, generically, one has a more complex system of coupled QDs instead of the conventional single-QD system. The electrostatic interaction between electrons tunnel through the single QD 4 with electrons in QDs 1, 2, and 3 renders the transport conditions for the QD 4 dependent on the population of the other three QDs (those with electrons of the opposite spin). As a result, in contrast to the simplest single-dot case (Figure 13c), not all transport gaps get closed in the CB map, as seen in Figure 15.

The origin of this feature is associated with the change of electron numbers in the (nonconducting) QDs 1, 2, and 3 by varying gate voltage. With changing gate voltage near the degeneracy point (where the free energies for $\{N\}_i$ and $\{N\}_i + 1_4$ should be equal), electron numbers N_1 , N_2 , or N_3 may change and hence affect the free energy in such a way that the transport condition for QD 4 in this range of V_g is no longer fulfilled at $V_{sd} \rightarrow 0$. This feature is fully consistent with the existence of weak spin-valve effect observed for some values of V_g , see Figures 3 and 4.

Interaction between Molecular Spins. In the previous section, it was shown that different configurations of molecular spins lead to different QDs systems with different free energies. Let us now discuss the orientation of the molecular spins that, in turn, determines the spin orientation of localized electrons on the ligands. We define the interaction energy between the spins of the electrons localized on the ligands as the free energy difference between antiparallel and parallel spin orientation,

$$E_{SS}(x_1, x_2, V_g) = F_{\uparrow\downarrow} - F_{\uparrow\uparrow} \quad (9)$$

The positions of the two molecules are again x_1 and x_2 . The interaction is caused by the repulsive Coulomb interaction in the presence of the Fano scattering in the energy region near the localized molecular state.

The interaction between localized spins shows a non-monotonous behavior as a function of the molecule positions, as depicted in Figure 16 (the interaction energy $E_{SS}(x_1, x_2, V_g)/E_C$ is presented in units of charging energy in this plot). Specifically, Figure 16 demonstrates the dependence of interaction energy E_{SS} on the position of the second molecule x_2 with the first molecule being fixed at $x_1 = 0.2$ and two distinct values of the dimensionless gate voltages (see plot). It is seen that for $U_g = 1$, the interaction between molecules, mediated by the conducting electrons in the CNT, is of the antiferromagnetic type independently of the position of the second molecule. This corresponds to the experimental observation of the low conductance in zero magnetic field (recall that for the antiparallel orientation of molecular spins

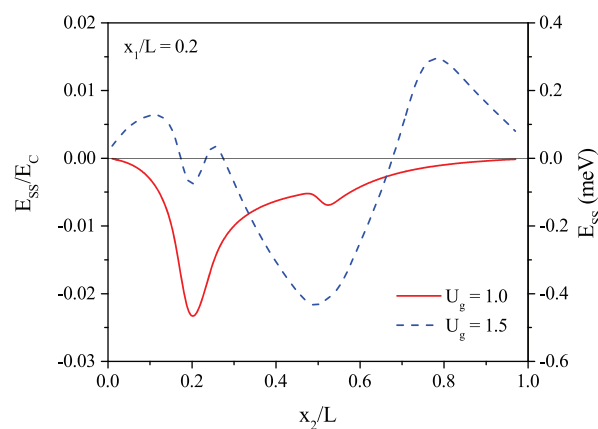


Figure 16. Interaction energy between localized spins as a function of position x_2 with fixed $x_1 = 0.2$ and $\kappa = 25$ for two values of the gate voltages. Negative (positive) values correspond to the antiferromagnetic (ferromagnetic) interaction.

both spin-up and spin-down electrons see two QDs, lower panel of Figure 12).

The typical interaction energy is of the order of $E_{SS} \sim 0.1 \div 0.2$ meV. At the same time, one sees that at different value of the gate voltage, $U_g = 1.5$, the effective spin–spin interaction between the molecules can be either antiferromagnetic or ferromagnetic, depending on the position of the second molecule. Figure 17 demonstrates the dependence of the

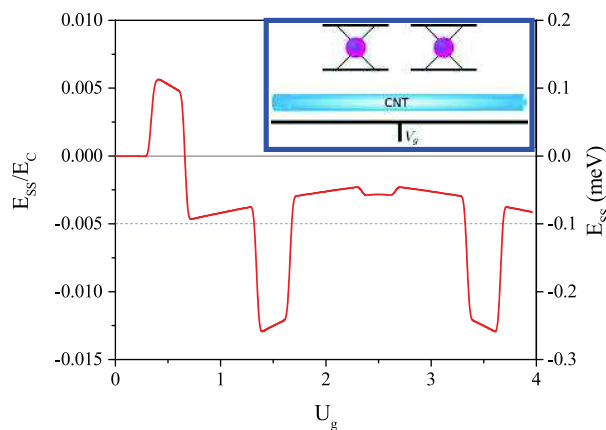


Figure 17. Interaction energy (red curve) between localized spins as a function of gate voltage U_g at fixed positions of the molecules, $x_1 = 0.2$ and $x_2 = 0.6$, and $\kappa = 25$. Negative (positive) values correspond to the antiferromagnetic (ferromagnetic) interaction. The dashed blue line corresponds to the interaction energy estimated from experiment. Inset: Schematics of the gated CNT with two TbPc_2 .

spin–spin interaction on the gate voltage for the fixed positions of the molecules, $x_1 = 0.2$ and $x_2 = 0.6$. Here, for almost all gate voltages the interaction is of the antiferromagnetic type and is in a good agreement with the experimental value of ~ 1 K which is indicated by the thin blue dashed line at Figure 17.

In finite magnetic fields, we can describe the CNT with SMMs by an effective spin Hamiltonian:

$$\hat{H}_{\text{eff}} = -\frac{E_{\text{SS}}}{2S^2}(\hat{S}_{1z}\hat{S}_{2z}) + A(\hat{S}_{1z}\hat{J}_{1z}) + A(\hat{S}_{2z}\hat{J}_{2z}) + \mu_B(g_T\hat{J}_1 + g_T\hat{J}_2 + g_S\hat{S}_1 + g_S\hat{S}_2)\cdot\mathbf{B} \quad (10)$$

where $g_T = 1.5$ and g_S are g -factors of terbium and localized electrons, respectively. To simplify the model, the terms describing the Zeeman energy of electrons localized on Pc can be omitted because of their small spin in comparison with the spin of terbium.

In this Hamiltonian, we assume that molecules have an easy axis in z direction. Due to the strong repulsive Coulomb interaction U_0 acting on the ligands of the molecule, the spin of the localized electrons $S_{1,2}$ is forced to align in z direction. With the effective Hamiltonian (eq 10), one can obtain the characteristic magnetic field at which the Zeeman energy exceeds the interaction energy E_{SS} , so that for stronger fields the molecular spins become parallel. Under the assumption of an applied magnetic field in z direction, the critical field is

$$B_c = \frac{E_{\text{SS}}}{\mu_B g_T J} \sim 0.2 \div 0.3 \text{ T} \quad (11)$$

This value is again in a good agreement with the experimental data showing the jumps of the conductance when the magnetic field is swept from -1 to 1 T, see Figure 2.

Conductance and GMR. For the analysis of the conductance in the regime of CB, one of the most powerful approaches is based on kinetic equations for the distribution function of the QD system.^{46,50} In our case, we address the regime of a finite source-drain voltage, where the kinetic equations cannot be solved exactly, in contrast to the linear regime of ref 46. At the same time, we focus on the low-temperature regime $T \ll \Delta$ which is relevant to the experiment. In this regime, the tunneling current can be obtained without solving kinetic equations by calculating the current-channel function $I(V_g, V_{\text{sd}})$ (Figures 14 and 15).

The antiparallel orientation of molecular spins corresponds to the vanishing magnetic field, while the parallel alignment of the spins is realized for magnetic fields above the critical one, $B > B_c$. We set the location of the molecules to $x_1 = 0.2$, $x_2 = 0.6$ and choose $\kappa = 25$. For antiparallel configuration, the conductance is strongly reduced in the region of the zero source-drain voltage due to Coulomb blockade. The transport gap $\delta V_{\text{sd}} \sim 1 \div 2$ meV that opens at zero B is clearly seen in Figure 14, in agreement with experimental observation, Figure 3.

As was pointed out above, not all transport gaps are closed for the parallel SMMs spin orientation. If the gate voltage corresponds to the closing of the gap in magnetic field above critical, a strong spin-valve effect (*i.e.*, the GMR) emerges, as in Figure 7. If the gap in magnetic field is open, it is typically smaller than the one at $B = 0$ (Figures 14 and 15), thus leading to a weak spin-valve effect, as in Figure 8 (a nonzero linear conductance is associated with finite temperature and level broadening). Thus, the V_g dependence of the strength of the spin-valve effect is explained by the developed theoretical model. The Coulomb interaction plays here a crucial role: without the CB effects, no transport gap would be possible when all SMM spins are aligned by the strong magnetic field.

The value of conductance can be estimated in the case of a few open channels, $I \sim 1$, which is realized for a small source-drain voltage $eV_{\text{sd}} \lesssim 0.3 E_C$. The molecule transparency \mathcal{T}_M is

much larger than the transparency of the barriers $\mathcal{T}_{L,R}$ (for energies not too close to the resonant energy, see Figure 10), yielding

$$\frac{G}{G_0} \sim \frac{\mathcal{T}_L \mathcal{T}_R}{\mathcal{T}_L + \mathcal{T}_R} \quad (12)$$

In Figure 18, the conductance as a function of source-drain voltage is shown for $U_g = 1.33$. The red dashed curve depicts

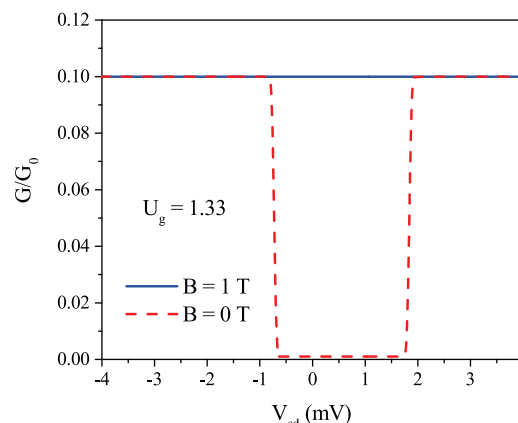


Figure 18. Linear conductance at zero T as a function of source-drain voltage at $U_g = 1.33$. The red dash curve corresponds to the absence of magnetic field (antiparallel molecules spins), the blue curve is associated with a finite magnetic field above the critical one, B_c (parallel molecules spins). The molecules are located at $x_1 = 0.2$, $x_2 = 0.6$ and $\kappa = 25$.

the conductance at $B = 0$ (antiparallel SMM spins) and the blue curve corresponds to a magnetic field above the critical magnetic field B_c (parallel SMM spins). The GMR effect, clearly seen in Figure 18, is due to the opening of the transport gap at zero magnetic field, see Figure 14, caused by the antiferromagnetic arrangement of molecular spins. The shift of the low-conductance window with respect to $V_{\text{sd}} = 0$ following from our model is again consistent with the experimental observations, Figure 7.

CONCLUSIONS

To conclude, we have presented experimental data and the theoretical model for the giant magnetoresistance effect (spin-valve effect) and Coulomb blockade in carbon nanotubes with side-attached molecular magnets. The proposed theoretical model explains qualitatively the giant magnetoresistance (*cf.* Figures 7 and 18) as well as the structure of Coulomb diamonds (*cf.* Figures 3, 4 and 14, 15) in the nonlinear transport in CNTs with side-attached SMMs.^{10,28,29} The same ideas and framework can be generalized to describe the spin-valve effect in other nanostructures.^{30,31} Below we summarize the main ingredients of the developed theory:

- The phthalocyanine ligands in TbPc₂ magnetic molecules have localized electronic states near the Fermi level ($S = 1/2$ state in Figure 1). These states are assumed to be well coupled to the electronic states of the nanotube.
- The exchange interaction between the electrons localized on the molecule and the electrons in the Tb shell combined with the strong repulsive Coulomb interaction on the ligands splits the localized states for spin-up and spin-down electrons (Figure 11).

- The Fano resonance induced by the side-attached molecules gives rise to a strong backscattering of electrons (Figure 10) in the energy window whose position depends on the relative orientation of electron and molecule spins, Figure 11.
- We consider a minimal model with two magnetic molecules attached to the carbon nanotube, where the Fano-resonance backscattering breaks up the nanotube into four quantum dots. Specifically, the nanotube is seen either as a single quantum dot and three quantum dots (parallel orientation of SMM spins) for spin-up and spin-down electrons, or as two quantum dots for each spin species of electrons (antiparallel SMM spins), Figure 12.
- Different energies of the configurations with parallel and antiparallel spins of the molecules lead to an effective magnetic interaction between the TbPc_2 spins, Figure 16. The sign of this interaction may depend on the positions of SMMs and can be tuned by the gate voltage.
- The spin-valve effect emerges for such gate voltages that provide the antiferromagnetic arrangement of the molecule spins. In zero external magnetic field, the spins of the molecules are antiparallel. Both spin-up and spin-down electrons tunnel through double quantum dots. The Coulomb blockade leads to a strongly suppressed conductance at zero source-drain voltage for all gate voltages, Figure 14.
- By applying external magnetic field, the spins of the molecules become parallel, when the Zeeman energy overcomes the effective antiferromagnetic coupling. For electrons with one spin orientation, the system acts as a triple quantum dot and the transport is blocked. However, electrons with the opposite spin see just a single quantum dot and the Coulomb-blockade gap closes at certain values of the gate voltage V_g , Figure 15. The configuration with a single quantum dot for electrons with this spin orientation provides then a lower resistance (Figure 18), thus leading to the spin-valve effect.
- The strength of the spin-valve effect depends on positions of molecules on the CNT and on the gate voltage through the charging energy of the system. For certain “resonant” values of the gate voltage, the effect is particularly strong and results in GMR.

Importantly, the developed theory predicts the existence of long-range interactions between SMMs mediated by the charging effects in a CNT. We have demonstrated that this effective spin–spin interaction (including its sign) depends on the gate voltage and positions of SMMs, see Figures 16 and 17. Furthermore, for the antiferromagnetic alignment of the SMM spins, the magnitude of the magnetoresistance also depends on the value of the gate voltage (cf. Figure 7 and Figure 8), thus giving rise to a *gate-controlled* spin-valve effect. This implies that the orientation of SMMs spins and the magnetic properties of supramolecular structures can be manipulated electrostatically by external gates, in particular, by engineering the nanostructures with multiple local gates.

The experimental realization of this effect in systems with controlled deposition of SMMs would be an important step in the direction of establishing molecular quantum spintronic devices in the community of nanoelectronics. In view of the fast evolution of the field of quantum systems, with such subfields as superconducting quantum circuits, trapped ions, quantum-

dot circuits, NV centers in diamond, and P-ions in Si being prominent examples, the ability of manipulating the localized degrees of freedom by electronic means becomes an urgent general challenge. For this purpose, supramolecular chemistry can supply powerful and affordable tools to tailor quite complex molecular devices, allowing proof-of-principle experiments on a “molecular quantum processor”.

METHODS

Single-wall carbon nanotubes of a diameter about 1.2 nm were grown by the laser ablation method. They were dispersed in 1–2 mL dichloroethane and sonicated for 1 h. A droplet of this suspension was deposited onto a degenerately doped p-type silicon wafer with a surface oxide of width about 450 nm. CNTs were located by atomic force microscopy with respect to predefined markers. Then, they are contacted with 50 nm-thick Pd by standard electron-beam lithography with a contact spacing of $L \sim 300$ nm.

TbPc_2 SMMs were synthesized as reported in ref 51. Supramolecular grafting was carried out by drop casting a solution of TbPc_2 diluted in dichloromethane with molarity $10^8 \text{ mol}\cdot\text{l}^{-1}$ onto the sample. After 5 s, the sample was rinsed in dichloromethane and dried under nitrogen flow. Residual dichloromethane was removed by a second rinse with isopropanol.

Samples with high resistance (>100 k Ω) at room temperature were selected. The conductance measurements were carried out in a He_3/He_4 dilution refrigerator with a base temperature of 30 mK. The magnetic field in the sample plane was provided by a magnet generating up to 1 T. Electrical measurements of interest were made using a Stanford Research Systems SR-830-DSP lock-in amplifier or an ADwin real-time data acquisition system. About 20% of all samples showed the magnetoresistance effect and were subsequently studied in detail.

ASSOCIATED CONTENT

Supporting Information

The Supporting Information is available free of charge on the ACS Publications website at DOI: 10.1021/acsnano.7b02014.

Technical details of the theoretical model, specifically: basics of the Fano resonance; dephasing for tunneling through a double-barrier system; transmission coefficient for two barriers with a Fano state in between; Coulomb blockade: free energy and current; Coulomb blockade: nanotube with two molecules (PDF)

AUTHOR INFORMATION

Corresponding Author

*E-mail: igor.gornyi@kit.edu.

ORCID

Mario Ruben: 0000-0002-7718-7016

Igor V. Gornyi: 0000-0002-9253-6691

Notes

The authors declare no competing financial interest.

ACKNOWLEDGMENTS

The authors thank N. Averkiev, A. Fediai, K. Fink, G. Finkelstein, D. Golosov, M. Grifoni, M. Katsnelson, M. Kiselev, A. Mirlin, D. Polyakov, and M. Urdampilleta for discussions. A.P.D. and I.V.G. are particularly grateful to P.M. Shmakov for collaboration on the initial stage of the project. This work was supported partly by the Russian Science Foundation (grant No 17-12-01182, I.V.K., A.P.D., I.V.G.), by Carl-Zeiss-Stiftung (J.K.), by the DFG TR 88 “3Met”, by the ANR “MolQuSpin”, and by Alexander von Humboldt foundation (W.W.).

REFERENCES

- (1) Gatteschi, D.; Sessoli, R.; Villain, J. *Molecular Nanomagnets; Mesoscopic Physics and Nanotechnology*, 5; Oxford Univ. Press: Oxford, 2006.
- (2) Rocha, A. R.; García-Suárez, V. M.; Bailey, S. W.; Lambert, C. J.; Ferrer, J.; Sanvito, S. Towards Molecular Spintronics. *Nat. Mater.* **2005**, *4*, 335–339.
- (3) Bogani, L.; Wernsdorfer, W. Molecular Spintronics Using Single-Molecule Magnets. *Nat. Mater.* **2008**, *7*, 179–186.
- (4) Sanvito, S. Molecular Spintronics. *Chem. Soc. Rev.* **2011**, *40*, 3336–3355.
- (5) Moreno Pineda, E.; Komeda, T.; Katoh, K.; Yamashita, M.; Ruben, M. Surface Confinement of TbPc₂-SMMs: Structural, Electronic and Magnetic Properties. *Dalton Trans.* **2016**, *45*, 18417–18433.
- (6) Bartolomé, J.; Luis, F.; Fernández, J. F. *Molecular Magnets: Physics and Applications; NanoScience and Technology*; Springer-Verlag: Berlin Heidelberg, 2014.
- (7) Jia, C.; Guo, X. Molecule-Electrode Interfaces in Molecular Electronic Devices. *Chem. Soc. Rev.* **2013**, *42*, 5642–5660.
- (8) Hueso, L. E.; Pruneda, J. M.; Ferrari, V.; Burnell, G.; Valdes-Herrera, J. P.; Simons, B. D.; Littlewood, P. B.; Artacho, E.; Fert, A.; Mathur, N. D. Transformation of Spin Information into Large Electrical Signals Using Carbon Nanotubes. *Nature* **2007**, *445*, 410–413.
- (9) Miyamachi, T.; Gruber, M.; Davesne, V.; Bowen, M.; Boukari, S.; Joly, L.; Scheurer, F.; Rogez, G.; Yamada, T. K.; Ohresser, P.; Beaupaire, E.; Wulfhekel, W. Robust Spin Crossover and Memristance Across a Single Molecule. *Nat. Commun.* **2012**, *3*, 938.
- (10) Urdampilleta, M.; Klyatskaya, S.; Cleuziou, J.-P.; Ruben, M.; Wernsdorfer, W. Supramolecular Spin Valves. *Nat. Mater.* **2011**, *10*, 502–506.
- (11) Zyazin, A. S.; van den Berg, J. W. G.; Osorio, E. A.; van der Zant, H. S. J.; Konstantinidis, N. P.; Leijnse, M.; Wegewijs, M. R.; May, F.; Hofstetter, W.; Danieli, C.; Cornia, A. Electric Field Controlled Magnetic Anisotropy in a Single Molecule. *Nano Lett.* **2010**, *10*, 3307–3311.
- (12) Galperin, M.; Nitzan, A. Molecular Optoelectronics: the Interaction of Molecular Conduction Junctions with Light. *Phys. Chem. Chem. Phys.* **2012**, *14*, 9421–9438.
- (13) Bairagi, K.; Iasco, O.; Bellec, A.; Kartsev, A.; Li, D.; Lagoute, J.; Chacon, C.; Girard, Y.; Rousset, S.; Miserque, F.; Dappe, Y. J.; Smogunov, A.; Barretau, C.; Boillot, M.-L.; Mallah, T.; Repain, V. Molecular-Scale Dynamics of Light-Induced Spin Cross-over in a Two-Dimensional Layer. *Nat. Commun.* **2016**, *7*, 12212.
- (14) Komeda, T.; Isshiki, H.; Liu, J.; Zhang, Y.-F.; Lorente, N.; Katoh, K.; Breedlove, B. K.; Yamashita, M. Observation and Electric Current Control of a Local Spin in a Single-Molecule Magnet. *Nat. Commun.* **2011**, *2*, 217.
- (15) Meded, V.; Bagrets, A.; Fink, K.; Chandrasekar, R.; Ruben, M.; Evers, F.; Bernand-Mantel, A.; Seldenthuis, J. S.; Beukman, A.; van der Zant, H. S. J. Electrical Control over the Fe(II) Spin Crossover in a Single Molecule: Theory and Experiment. *Phys. Rev. B: Condens. Matter Mater. Phys.* **2011**, *83*, 245415.
- (16) Jia, C.; Migliore, A.; Xin, N.; Huang, S.; Wang, J.; Yang, Q.; Wang, S.; Chen, H.; Wang, D.; Feng, B.; Liu, Z.; Zhang, G.; Qu, D.-H.; Tian, H.; Ratner, M. A.; Xu, H. Q.; Nitzan, A.; Guo, X. Covalently Bonded Single-Molecule Junctions with Stable and Reversible Photoswitched Conductivity. *Science* **2016**, *352*, 1443–1445.
- (17) Ishikawa, N.; Sugita, M.; Okubo, T.; Tanaka, N.; Iino, T.; Kaizu, Y. Determination of Ligand-Field Parameters and *f*-Electronic Structures of Double-Decker Bis(phthalocyaninato)lanthanide Complexes. *Inorg. Chem.* **2003**, *42*, 2440–2446.
- (18) Ishikawa, N.; Sugita, M.; Tanaka, N.; Ishikawa, T.; Koshihara, S.-y.; Kaizu, Y. Upward Temperature Shift of the Intrinsic Phase Lag of the Magnetization of Bis(phthalocyaninato)terbium by Ligand Oxidation Creating an *S* = 1/2 Spin. *Inorg. Chem.* **2004**, *43*, 5498–5500.
- (19) Christou, G.; Gatteschi, D.; Hendrickson, D. N.; Sessoli, R. Single-Molecule Magnets. *MRS Bull.* **2000**, *25*, 66–71.
- (20) Cornia, A.; Costantino, A. F.; Zobbi, L.; Caneschi, A.; Gatteschi, D.; Mannini, M.; Sessoli, R. In *Single-Molecule Magnets and Related Phenomena*; Winpenny, R., Ed.; Springer Berlin Heidelberg: Berlin, Heidelberg, 2006; pp 133–161.
- (21) Katoh, K.; Yoshida, Y.; Yamashita, M.; Miyasaka, H.; Breedlove, B. K.; Kajiwara, T.; Takaishi, S.; Ishikawa, N.; Isshiki, H.; Zhang, Y. F.; Komeda, T.; Yamagishi, M.; Takeya, J. Direct Observation of Lanthanide(III)-Phthalocyanine Molecules on Au(111) by Using Scanning Tunneling Microscopy and Scanning Tunneling Spectroscopy and Thin-Film Field-Effect Transistor Properties of Tb(III)- and Dy(III)-Phthalocyanine Molecules. *J. Am. Chem. Soc.* **2009**, *131*, 9967–9976.
- (22) Fleury, B.; Catala, L.; Huc, V.; David, C.; Zhao Zhong, W.; Jegou, P.; Baraton, L.; Palacin, S.; Albouy, P.-A.; Mallah, T. A New Approach to Grafting a Monolayer of Oriented Mn₁₂ Nanomagnets on Silicon. *Chem. Commun.* **2005**, 2020–2022.
- (23) Naitabdi, A.; Bucher, J.-P.; Gerbier, P.; Rabu, P.; Drillon, M. Self-Assembly and Magnetism of Mn₁₂ Nanomagnets on Native and Functionalized Gold Surfaces. *Adv. Mater.* **2005**, *17*, 1612–1616.
- (24) Coronado, E.; Forment-Aliaga, A.; Gaita-Ariño, A.; Giménez-Saiz, C.; Romero, F. M.; Wernsdorfer, W. Polycationic Mn₁₂ Single-Molecule Magnets as Electron Reservoirs with *S* > 10 Ground States. *Angew. Chem., Int. Ed.* **2004**, *43*, 6152–6156.
- (25) Bogani, L.; Cavigli, L.; Gurioli, M.; Novak, R.; Mannini, M.; Caneschi, A.; Pineider, F.; Sessoli, R.; Clemente-León, M.; Coronado, E.; Cornia, A.; Gatteschi, D. Magneto-Optical Investigations of Nanostructured Materials Based on Single-Molecule Magnets Monitor Strong Environmental Effects. *Adv. Mater.* **2007**, *19*, 3906–3911.
- (26) Ishikawa, N.; Sugita, M.; Ishikawa, T.; Koshihara, S.-y.; Kaizu, Y. Mononuclear Lanthanide Complexes with a Long Magnetization Relaxation Time at High Temperatures: A New Category of Magnets at the Single-Molecular Level. *J. Phys. Chem. B* **2004**, *108*, 11265–11271.
- (27) Mannini, M.; Pineider, F.; Sainctavit, P.; Danieli, C.; Otero, E.; Sciancalepore, C.; Talarico, A. M.; Arrio, M.-A.; Cornia, A.; Gatteschi, D.; Sessoli, R. Magnetic Memory of a Single-Molecule Quantum Magnet Wired to a Gold Surface. *Nat. Mater.* **2009**, *8*, 194–197.
- (28) Urdampilleta, M.; Klyatskaya, S.; Ruben, M.; Wernsdorfer, W. Landau-Zener Tunneling of a Single Tb³⁺ Magnetic Moment Allowing the Electronic Read-out of a Nuclear Spin. *Phys. Rev. B: Condens. Matter Mater. Phys.* **2013**, *87*, 195412.
- (29) Urdampilleta, M.; Nguyen, N.-V.; Cleuziou, J.-P.; Klyatskaya, S.; Ruben, M.; Wernsdorfer, W. Molecular Quantum Spintronics: Supramolecular Spin Valves Based on Single-Molecule Magnets and Carbon Nanotubes. *Int. J. Mol. Sci.* **2011**, *12*, 6656.
- (30) Candini, A.; Klyatskaya, S.; Ruben, M.; Wernsdorfer, W.; Affronte, M. Graphene Spintronic Devices with Molecular Nanomagnets. *Nano Lett.* **2011**, *11*, 2634–2639.
- (31) Aurich, H.; Baumgartner, A.; Freitag, F.; Eichler, A.; Trbovic, J.; Schönenberger, C. Permalloy-based Carbon Nanotube Spin-Valve. *Appl. Phys. Lett.* **2010**, *97*, 153116.
- (32) Hammar, H.; Fransson, J. Time-dependent Spin and Transport Properties of a Single-Molecule Magnet in a Tunnel Junction. *Phys. Rev. B: Condens. Matter Mater. Phys.* **2016**, *94*, 054311.
- (33) Aligia, A. A.; Roura-Bas, P.; Florens, S. Impact of Capacitance and Tunneling Asymmetries on Coulomb Blockade Edges and Kondo Peaks in Nonequilibrium Transport through Molecular Quantum Dots. *Phys. Rev. B: Condens. Matter Mater. Phys.* **2015**, *92*, 035404.
- (34) Luo, G.; Park, K. Magnetic-anisotropy-induced Spin Blockade in a Single-Molecule Transistor. *Phys. Rev. B: Condens. Matter Mater. Phys.* **2016**, *94*, 174412.
- (35) Płomińska, A.; Weymann, I. Nontrivial Magnetoresistive Behavior of a Single-wall Carbon Nanotube with an Attached Molecular Magnet. *Phys. Rev. B: Condens. Matter Mater. Phys.* **2015**, *92*, 205419.

- (36) Hong, K.; Kim, W. Y. Fano-Resonance-Driven Spin-Valve Effect Using Single-Molecule Magnets. *Angew. Chem., Int. Ed.* **2013**, *52*, 3389–3393.
- (37) Fano, U. Effects of Configuration Interaction on Intensities and Phase Shifts. *Phys. Rev.* **1961**, *124*, 1866–1878.
- (38) Miroschnichenko, A.; Flach, S.; Kivshar, Y. Fano Resonances in Nanoscale Structures. *Rev. Mod. Phys.* **2010**, *82*, 2257–2298.
- (39) Nazarov, Y. V.; Blanter, Y. M. *Quantum Transport: Introduction to Nanoscience*, 1st ed.; Cambridge Univ. Press: Cambridge, 2009.
- (40) Thiele, S.; Vincent, R.; Holzmann, M.; Klyatskaya, S.; Ruben, M.; Balestro, F.; Wernsdorfer, W. Electrical Readout of Individual Nuclear Spin Trajectories in a Single-Molecule Magnet Spin Transistor. *Phys. Rev. Lett.* **2013**, *111*, 037203.
- (41) Vincent, R.; Klyatskaya, S.; Ruben, M.; Wernsdorfer, W.; Balestro, F. Electronic Read-out of a Single Nuclear Spin Using a Molecular Spin Transistor. *Nature* **2012**, *488*, 357–360.
- (42) Thiele, S.; Balestro, F.; Ballou, R.; Klyatskaya, S.; Ruben, M.; Wernsdorfer, W. Electrically Driven Nuclear Spin Resonance in Single-Molecule Magnets. *Science* **2014**, *344*, 1135–1138.
- (43) Ganzhorn, M.; Klyatskaya, S.; Ruben, M.; Wernsdorfer, W. Strong Spin-Phonon Coupling Between a Single-Molecule Magnet and a Carbon Nanotube Nanoelectromechanical System. *Nat. Nanotechnol.* **2013**, *8*, 165–169.
- (44) Ganzhorn, M.; Klyatskaya, S.; Ruben, M.; Wernsdorfer, W. Quantum Einstein-de Haas Effect. *Nat. Commun.* **2016**, *7*, 11443.
- (45) Vitali, L.; Fabris, S.; Conte, A. M.; Brink, S.; Ruben, M.; Baroni, S.; Kern, K. Electronic Structure of Surface-supported Bis-(phthalocyaninato) terbium(III) Single Molecular Magnets. *Nano Lett.* **2008**, *8*, 3364–3368.
- (46) Beenakker, C. W. J. Theory of Coulomb-Blockade Oscillations in the Conductance of a Quantum Dot. *Phys. Rev. B: Condens. Matter Mater. Phys.* **1991**, *44*, 1646–1656.
- (47) Lopes, M.; Candini, A.; Urdampilleta, M.; Reserbat-Plantey, A.; Bellini, V.; Klyatskaya, S.; Marty, L.; Ruben, M.; Affronte, M.; Wernsdorfer, W.; Bendiab, N. Surface-Enhanced Raman Signal for Terbium Single-Molecule Magnets Grafted on Graphene. *ACS Nano* **2010**, *4*, 7531–7537.
- (48) Sapmaz, S.; Jarillo-Herrero, P.; Kong, J.; Dekker, C.; Kouwenhoven, L. P.; van der Zant, H. S. J. Electronic Excitation Spectrum of Metallic Carbon Nanotubes. *Phys. Rev. B: Condens. Matter Mater. Phys.* **2005**, *71*, 153402.
- (49) van der Wiel, W. G.; De Franceschi, S.; Elzerman, J. M.; Fujisawa, T.; Tarucha, S.; Kouwenhoven, L. P. Electron Transport Through Double Quantum Dots. *Rev. Mod. Phys.* **2002**, *75*, 1–22.
- (50) Matveev, K. A.; Glazman, L. I.; Baranger, H. U. Coulomb Blockade of Tunneling Through a Double Quantum Dot. *Phys. Rev. B: Condens. Matter Mater. Phys.* **1996**, *54*, 5637–5646.
- (51) Klyatskaya, S.; Galán Mascarós, J. R.; Bogani, L.; Hennrich, F.; Kappes, M.; Wernsdorfer, W.; Ruben, M. Anchoring of Rare-Earth-Based Single-Molecule Magnets on Single-Walled Carbon Nanotubes. *J. Am. Chem. Soc.* **2009**, *131*, 15143–15151.